Electronic Supplementary Material (ESI) for Environmental Science: Nano.

Dynamic Aqueous Transformations of Lithium Cobalt Oxide Nanoparticle Induce Distinct Oxidative Stress Responses of *B. subtilis*

Metti K. Gari[a], Paul Lemke[a], Kelly H. Lu[a], Elizabeth D. Laudadio[b], Austin H. Henke[b], Curtis M. Green[b], Thomas Pho[a, 1], Khoi Nguyen L. Hoang[c], Catherine J. Murphy[c], Robert J. Hamers[b], Z. Vivian Feng[a*]

Supporting Information

Table of Contents:

H_2O_2 diffusion experiment:

The use of fluorescent probes is a common and effect approach to detecting ROS.[1] However, one of many possible errors that can arise when using such a probe molecule is false-positive detection via the probe reacting at a potentially catalytic surface, such as $LiCoO_2$ nanoparticles.[2] To ensure that positive results of the amplex red assay were due to free H_2O_2 and not transformation of amplex red to resorufin on the nanoparticle surface, we performed diffusion assays with $LiCoO_2$ dissolution. We chose the amplex red assay because preliminary experiments identified H_2O_2 as the primary ROS generated. A solution of 100 µM amplex red and 0.1 unit·mL-1 horseradish peroxidase (AR-HRP) and a standard solution of 1 µM H_2O_2 were each prepared in minimal media with dextrose. These concentrations were chosen based on prior work,[3] to maximize H_2O_2 capture and produce fluorescence within a reasonable range. Experiments were performed with/without $LiCoO_2$ particles, with/without spiked H_2O_2 (as a positive control), and were each performed in at least duplicate. Figure X shows the device prepared for each sample to spatially separate the $LiCoO_2$ nanoparticles from the AR-HRP solution using a finely porous hydrophobic filter membrane (MF-Millipore, 25 nm pore size, 13 mm diameter). First, $LiCoO_2$ particles were pressed into indium foil on a copper plate to immobilize them. In the case of no- $LiCoO_2$ controls, indium pressed on copper was used. Next, 10 µL of minimal media with dextrose with/without 1 µM H_2O_2 (no AR-HRP) was added on the particle plate to promote dissolution, and in the case of H_2O_2 to simulate if H_2O_2 were produced by the particles. Then, a filter membrane disk is added on the plate, followed by an o-ring. 100 µL of the AR-HRP solution was added within the o-ring cavity, above the filter membrane. Finally, the o-ring is capped with a glass slide and sealed with a clamp. We allowed the particles to dissolve unstirred for 1 hr, disassembled the device, and removed 50 µL from within the o-ring above the membrane. This extracted solution was diluted into 1 mL of minimal media with dextrose and analyzed by fluorescence spectroscopy with conditions similar to those used previously.[3] Intensity at the emission peak maximum (~582 nm) was used for quantification, with the AR-HRP-only negative control serving as a baseline. Approximate quantification of unknown H_2O_2 generated from $LiCoO_2$ samples was possible due to the known quantity of spiked H_2O_2 (i.e. standard addition).

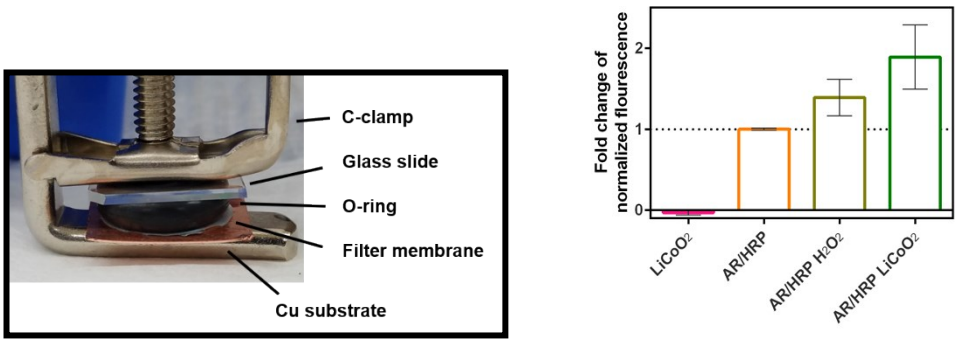

Figure S1. Assembled device for diffusion assay of Amplex Red with $LiCoO_2$ dissolution. $LiCoO_2$ nanoparticles are between the filter membrane and the copper substrate. The AR-HRP solution removed for analysis is housed within the o-ring, above the filter membrane. The resulting fluorescence intensities are measured at 580 nm from diffused H_2O_2.

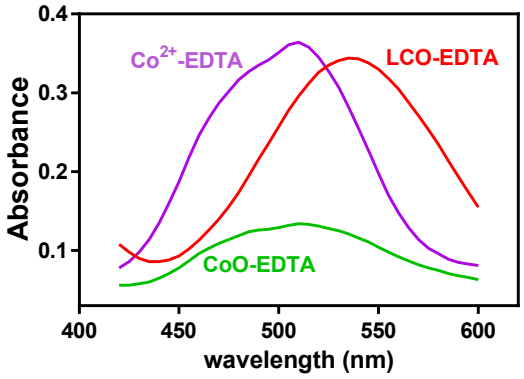

Figure S2. Spectrophotometric characterization of $LiCoO_2$ dissolution in the presence of 10 mM EDTA in acidic medium. Co(II)-EDTA complex absorbs at 490 nm, while Co(III)-EDTA is red-shifted to 540 nm.[6] CoO nanoparticle was used as a control to produce Co(II)-EDTA complex.

Characterization of lithium cobalt oxide nanoparticles after exposure in growth medium

To complement the abiotic ROS generation and ion release, we examined the morphological and surface compositional changes of the $LiCoO_2$ nanoparticles after 1-hr and 48-hr of suspensions in solution. After the desired incubation period in minimal medium, $LiCoO_2$ particles were recollected for analysis with XPS via centrifugation (14,104 ×*g*, 5 min). The pellet was redispersed in 1 mL ultrapure water, and re-isolating via centrifugation again. The supernatant was removed and the pellet was dried under vacuum at 30 °C overnight. The dried pellet was pressed into indium foil on a copper foil backing for XPS analysis. Analysis was done using a Thermo Fisher Scientific K-Alpha X-ray Photoelectron Spectrometer using at a 45° photoelectron takeoff angle. During analysis, the C(1s), Ca(2p), Cl(2p), Co(2p), K(2p), Li(1s), Mg(1s), N(1s), Na(1s), O(1s), P(2p) and S(2p) regions were monitored. XPS spectra were fit using CasaXPS software. No appreciable signal was observed for the Cl(2p), K(2p), Na(1s), or S(2p) regions. Atomic coverages of the adsorbates were estimated as described in the Supporting Information. Coverage of carbon was separated into total carbon (area of entire region) and oxidized carbon (area of only higher binding energy peaks).

For STEM images of transformed $LiCoO_2$ nanoparticles, the medium-exposed samples were centrifuged at 14,100 xg for 3 minutes and redispersed in 1.0 mL of water, and further diluted 100x before drop-casted on a TEM grid (Ted Pella copper grid with carbon type-B 300 mesh). The samples were characterized on a FEI Themis Z operated at 300 keV with a Schottky electron emitter, an electron energy monochromator, and a fifth order probe spherical aberration corrector.

Fig S2a-2d show SEM and STEM micrographs after either 1 hr or 48 hr exposure to the medium. To assess if any solution species were adsorbed to the particle surfaces, both XPS and EDS were employed to characterize the surface composition of the particles after exposure to the medium. XPS shows coverages of ≤1atoms/nm^2 of each Ca, Mg, N, and P on the nanoparticle surfaces, which is commensurate with sub-monolayer coverages (detailed analysis and sample spectra shown in Fig S3). The surface elemental compositions do not change significantly over time (Fig S2e). Similar observations were made in EDS measurements (data not shown).

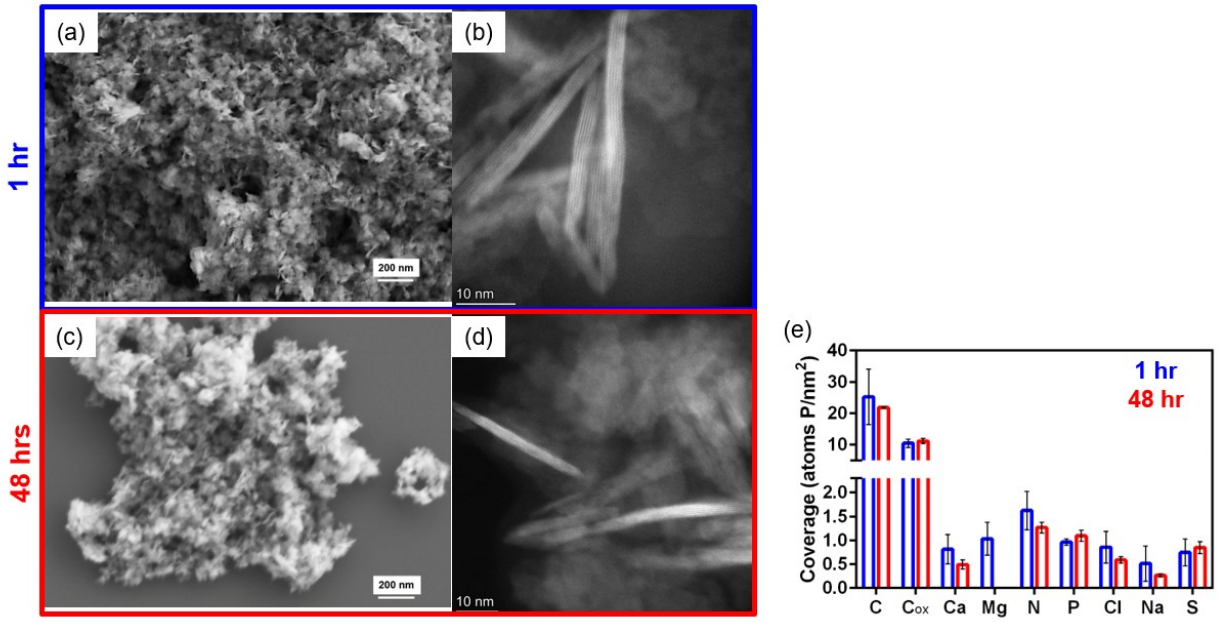

Figure S3. SEM and STEM images showing $LiCoO_2$ nanoparticle morphology after 1-hr (a-b) and 48-hr (c-d) suspension in growth medium. (e) XPS elemental characterizations of surface composition after medium exposure.

XPS surface adsorbate calculations and sample XPS spectra.

Atomic coverage of adsorbates (ads) was estimated using the following equation:

$$Coverage = \frac{A_{ads}}{A_{Co,2p}} \times \frac{SF_{Co,2p}}{SF_{ads}} \times \frac{Scans_{Co,2p}}{Scans_{ads}} \times \rho_{Co,2p} \times \lambda_{Co,2p} \times \cos\theta$$

Where A = peak area, SF = atomic sensitivity factor, ρ = density of cobalt in $LiCoO_2$, λ = inelastic mean free path (IMFP) of a cobalt photoelectron emitted from $LiCoO_2$, calculated from the NIST database[4] via the TPP-2M equation,[5] and θ = angle of the analyzer to the surface normal, 45°. This equation assumes a layer of absorbates thin relative to the IMFP, which is valid given our results. Values for each variable are listed in the table below, and representative spectra for each region monitored at the 1-hr time point.

Element	C	Ca	Co	Mg	N	P
SF	1	5.97	18.23529	14.94	1.676	1.352941
# Scans	30	30	10	30	30	50

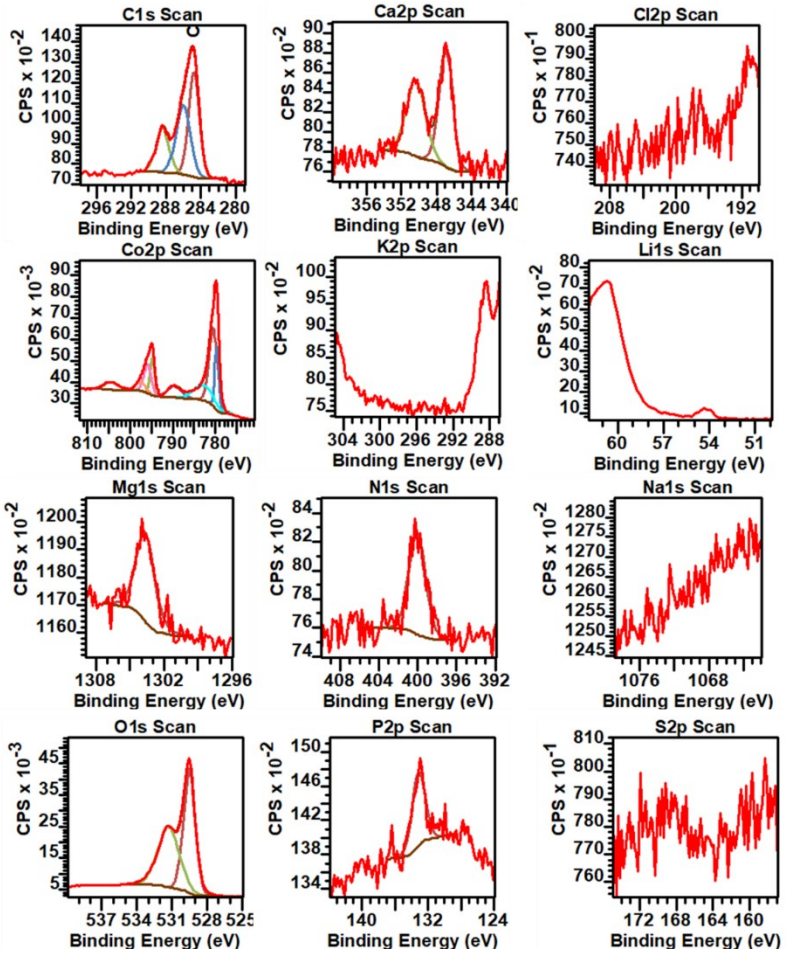

Figure S4. Sample XPS spectra.

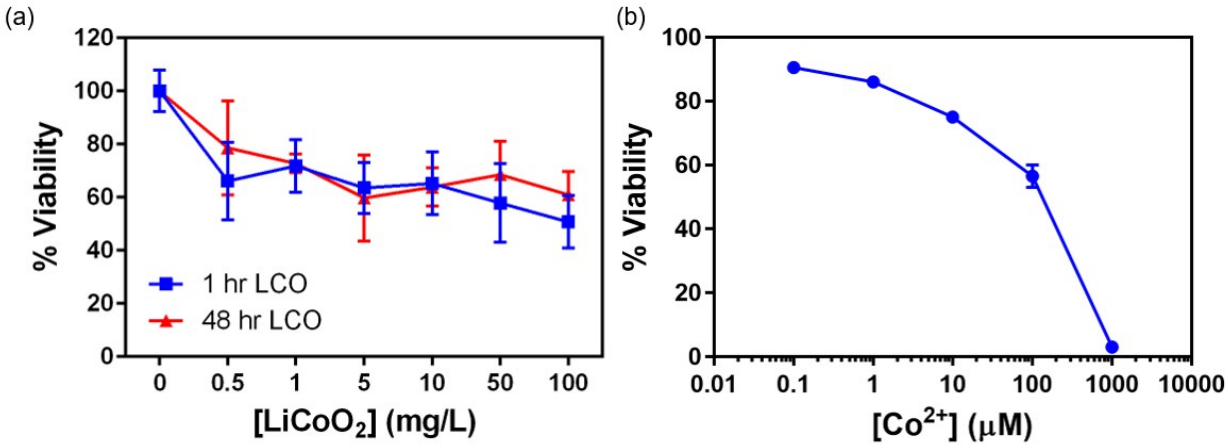

Figure S5. Growth based viability dose-dependent curves for *B. subtilis* in minimal medium with dextrose upon exposure to (a) $LiCoO_2$ nanosheets, and (b) Co^{2+} ions.

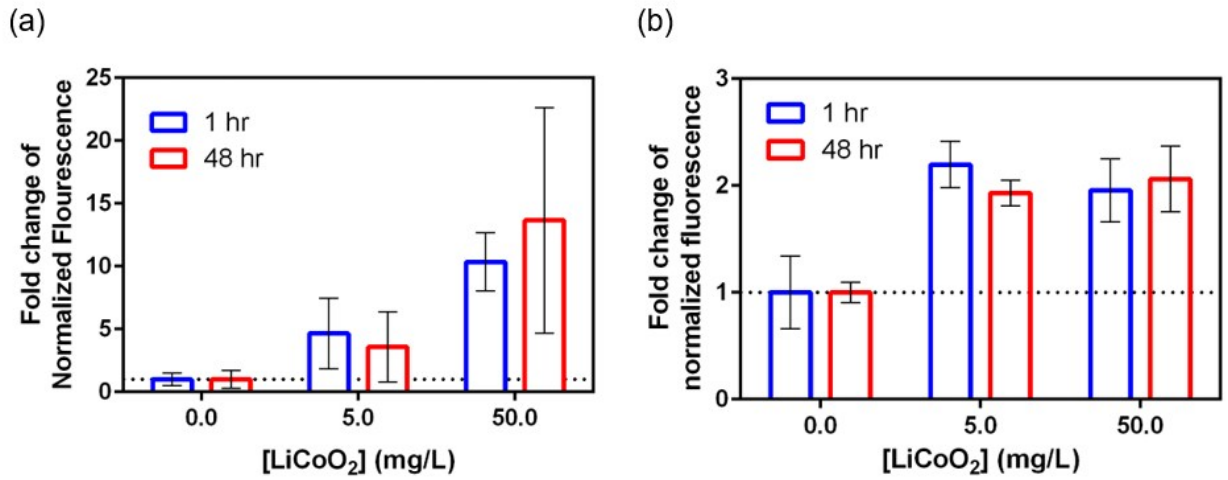

Figure S6. Intracellular ROS detection in *B. subtilis* induced by $LiCoO_2$ nanoparticle suspensions monitored with DCF-DA dye (a) and DHE (b).

ROS-Glo™ assay for decomposition of intracellular H_2O_2

Bacterial cells were harvested by centrifugation (3000 xg for 10 minutes). Cells were then resuspended and adjusted to have an absorbance of 0.6 at 600 nm (OD_{600}). 70 µL of cells at the desired density were added to 96-well plates. 20 µL of H_2O_2 Substrate solution was added to cells and mixed to give a final well volume of 100 µL, and a final H_2O_2 Substrate concentration to be 25 µM. Cells were placed on an incubator at 37 ^oC for 30 minutes. 100 µL of ROS-Glo™ Detection Solution was added to each well. Relative luminescence unit was measured using a plate reader.

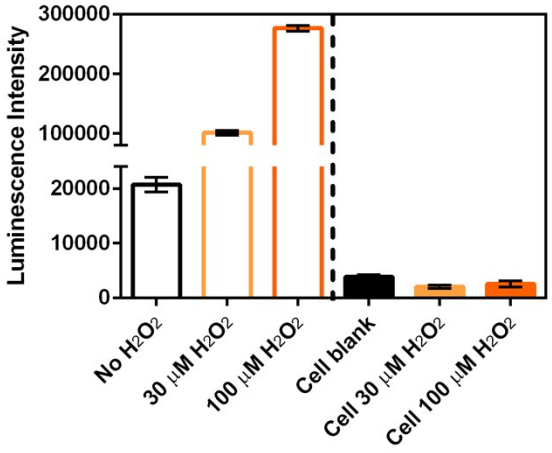

Figure S7. H_2O_2 decomposition in *B. subtilis* monitored by the ROSGlo™ assay.

Experimental procedure for RNA extraction from *B. subtilis* for qPCR study

A Direct-zol™ RNA MiniPrep kit (Zymo Research, Irvine, CA) was used to extract RNA from *Bacillus subtilis* according to the manufactural procedure. From frozen exposed cell, bacterial pellets were thawed and resuspended in RNAzol® RT solution (Molecular Research Center, Inc.). The bacterial cells were homogenized using FastPrep-24™ 5G Homogenizer (MP Biomedicals) at 10 M/S, 5 cycle of 300 seconds, pause of 100 seconds between cycle with 0.1 mm RNAse free glass beads (Next Advance Inc., GB01-RNA) in RNAzol® RT solution. RNA was then extracted from lysed cells with an on-column DNase I treatment at 30 ^{o}C for 30 minutes, and eluted with nuclease-free water from the column by spinning at 13,000 xg for 1 minute. The centrifugation step was repeated with RNA wash buffer and DNase and RNase free H_2O two more times. The purified RNA was characterized and quantified using a NanoDrop™ Microvolume UV-vis spectrophotometer using the nucleic acid ratio of 260/280. The RNA samples were then stored at -80˚C until reverse transcription.

Table S1. Genes functions and primers used in gene expression study.

Target Gene	Forward Primer (5'-3')	Reverse Primer (5'-3')	Protein Product	Function	Gene ID	Accession Number
katA	GCT CCG GTT GGA GAT AAT CAA	GAA CAC GTT CTC GGT TGA AAT G	Vegetative catalase 1	Oxidative stress	939240	NP_388762.2
ahpC	GAC CCA TCT CAA ACG ATC TCT C	GAT ACC GCC TGC ATT GAT TTC	Alkyl hydroperoxide reductase subunit C	Oxidative stress	938147	NP_391889.1
ohrA	AGA CAG AGG TTA CAGC AAA TGT	CTG ATG CAC TGA CTC CTT CTC	Peroxiredoxin	Oxidative stress	939848	NP_388753.1
tpx	GTG CTG ACTA ACA GCC TTG A	GTG CAT CAC AAA CAC CTG TAT C	Thiol peroxidase	Oxidative stress	938727	NP_390827.1
perR	GCC TTA GAA ACG TTG AAG GAA AC	GCT GTT GGA TGA GCC ATA GA	Transcriptional regulator (Fur family)	Oxidative stress	939227	NP_390381.3
mrgA	CTC CAC CGT TTC CAT TGG TAT	AGC GAT GGT ATC CAC TGT TTC	Metalloregulation DNA-binding stress protein	Oxidative stress	938592	NP_391178.1
sodA	GCT TGT TGT GAA CAA CGG TAA A	CTC CCA AAC GTC AAG ACC TAA G	Superoxide dismutase	Oxidative stress	938052	NP_390302.1
fur	CGT TAC GAC CTT CGG AAA GAG	CTT CCA CGT CTT CAA GCA AAT C	Transcriptional repressor of iron uptake	Oxidative stress	937688	NP_390233.2
czcD	ATT ATG ATG AGT GGC GGA GAT AC	GAG CCG AGC ATA TCG CTT ATT A	cadmium, cobalt and zinc/H	Metal homeostasis	937630	NP_390542.1
mutM	GTA GAG ATC AGA TGG CCG AAT ATC	CCG ATG GAC TGT ATC GTT TCT C	Endonuclease III/thymine glycol DNA glycosylase	DNA repair & metabolism	936741	NP_390786.2
recJ	CTG GAA GAT GTC CGC AAG ATA G	CCT TCT TGA AGC TCG CCTTTA	Single-stranded-dna-specific exonuclease RecJ	DNA repair & metabolism	937538	NP_390640.1
ruvA	CTT GAA GAA GCA CTT GAA GCC	GTC TGT TGT CAG CCC AAT TTC	Holliday junction ATP-dependent DNA helicase RuvA	DNA repair & metabolism	937829	NP_390652.1
lexA	TGC GAT GAC AGA AGA TGA TGA A	CGC CAA TCA CTT TCC CTA GAA	Lexa repressor	DNA repair & metabolism	939564	NP_389668.1
recU	CCG CTT TCG ACC AGG TTT AT	AGC TGT TTC TTC CAA CTC ATC T	holliday junction resolvase RecU	DNA repair & metabolism	939039	NP_390112.1
radA	GTA CCG CTG AGC TGA TGA AA	AGT CTC GGA CCT GCA ATA GA	ATP-dependent protease	Housekeeping	936872	NP_390542.1

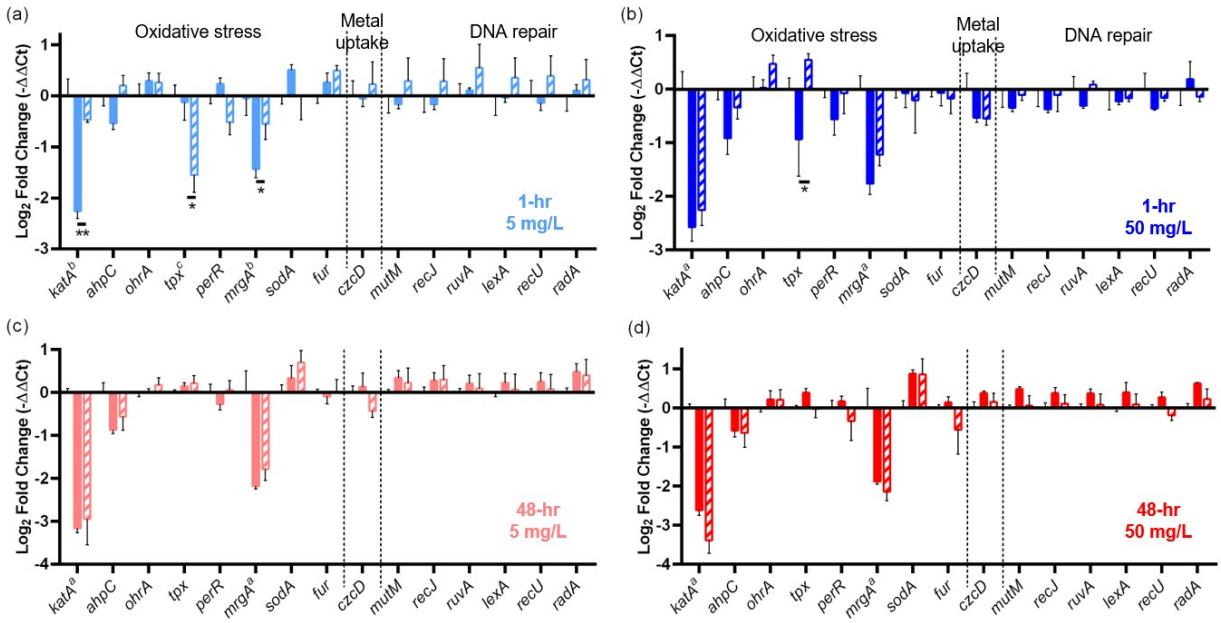

Figure S8. Quantitative PCR analysis of changes in gene expression in *B. subtilis* upon exposure to $LiCoO_2$ and Co^{2+}.

References:

(1) Fernández-Castro, P.; Vallejo, M.; San Román, M. F.; Ortiz, I. Insight on the Fundamentals of Advanced Oxidation Processes: Role and Review of the Determination Methods of Reactive Oxygen Species. *Journal of Chemical Technology and Biotechnology*. **2015**, 796–820.

(2) Bartosz, G. Use of Spectroscopic Probes for Detection of Reactive Oxygen Species. *Clinica Chimica Acta*. **2006**, 53–76.

(3) Zhao, B, Summers F. A, and Mason, R. P. Photooxidation of Amplex Red to Resorufin: Implications of Exposing the Amplex Red Assay to Light. *Free Radic. Biol. Med.* **2012**, *53*, 1080–1087.

(4) Powell, C. J.; Jablonski, A. *N IST Standard Reference Database 82 NIST Electron Effective-Attenuation-Length Database*; **2011**.

(5) Tanuma, S.; Powell, C. J.; Penn, D. R. Calculation of Electron Inelastic Mean Free Paths (IMFPs) VII. Reliability of the TPP-2M IMFP Predictive Equation. *Surf. Interface Anal.* **2003**, *35*, 268–275.

(6) Paraneeiswaran, A.; Shukla, S. K.; Sathyaseelan, V. S.; Rao, T. S. A Spectrophotometric Method for the Determination Co-EDTA Complexes. *Int. J. Appl. Sci. Biotechnol.* **2015**, *3*, 584–587.